

Ultimate resolution of indefinite metamaterial flat lenses

Jessica Bénédicto,^{1,2} Emmanuel Centeno,^{1,2} Rémi Pollès,^{2,3} and Antoine Moreau^{1,2}

¹*Clermont Université, Université Blaise Pascal, Institut Pascal, Boîte Postale 10448, F-63000 Clermont-Ferrand, France*

²*CNRS, UMR 6602, Institut Pascal, F-63177 Aubière, France*

³*Clermont Université, Université d'Auvergne, Boîte Postale 10448, F-63000 Clermont-Ferrand, France*

(Received 16 July 2013; published 31 December 2013)

We propose an approach allowing a systematic optimization of lenses based on hyperbolic metamaterials. The lensing properties of these highly anisotropic materials are summed up in a complex effective index extracted from the complex dispersion relation. The analytical expression of this effective index in the homogenization regime or its direct computation from the Bloch band diagram in the resonant regime leads to hyperbolic metamaterials that outperform the state-of-art flat lenses. We show that feasible metal-dielectric multilayers provide superresolved images for visible light (around 400 nm) even when fully taking absorption into account.

DOI: [10.1103/PhysRevB.88.245138](https://doi.org/10.1103/PhysRevB.88.245138)

PACS number(s): 42.25.Fx, 78.20.Ci, 78.67.Pt

I. INTRODUCTION

Since the seminal work of Pendry, who proposed a perfect lens of unlimited resolution, intensive efforts have been made to realize reliable metamaterials that could make this concept effective.¹ Beating the optical diffraction limit requires conceiving bulk metamaterials presenting both electric and magnetic permittivities (ϵ and μ) equal to -1 . These slabs of -1 refractive index are, however, particularly difficult to realize at optical frequencies since their building blocks (split-ring resonators, wires) are not sizable at the nanometer scale.² An alternative approach has recently emerged with feasible metal-dielectric multilayers, referred to as indefinite metamaterials, which operate at ultraviolet frequencies.³ These highly anisotropic media present hyperbolic photonic dispersion surfaces in the k space, which induces enhanced optical properties⁴⁻⁸ (Fig. 1). Consequently, both propagating and evanescent waves emitted by a source decompose into propagating waves in the hyperbolic medium, so that the subwavelength details are efficiently transported through the lens. This principle has been experimentally demonstrated in the far-field space with a hyperlens that presents a spherical shape.⁹⁻¹¹ Planar indefinite hyperbolic metamaterials have also been theoretically predicted to form subwavelength images bonded at the output interface of the lens when the canalization regime is reached.^{12,13} Other results have, moreover, shown that light focalization is also possible in the near field, and a lens equation for these hyperbolic lenses has been derived.¹⁴⁻¹⁷ Other progress towards negative-index metamaterials has been reported theoretically and demonstrated experimentally with coupled plasmonic waveguide structures that resemble indefinite metamaterials.^{18,19} The latter results have, in particular, shown that these metamaterials behave as -1 effective index flat lenses that make images for ultraviolet light.¹⁹ This effective index has been evidenced by tracking the refracted angles of a beam launched for various incident angles through a stack of silver and TiO₂ thin films. According to the authors, subwavelength resolution has not been achieved because of the optical losses, which are known to reduce the efficiency of metamaterials lenses.

However, very little is known so far on the exact role of optical losses on the optimal optical resolution of indefinite metamaterials lenses, and to our knowledge, there is no

theoretical model that allows a systematic optimization of such systems. In this work, we develop a method that allows us to extract a complex effective index $\bar{n} = n + i\kappa$ for indefinite metamaterials. The usual homogenization techniques start from the constituents of the composite materials and deduce the effective index required to determine the photon dispersion.²⁰⁻²⁴ These bottom-up approaches, restricted to the long-wavelength limit, lead us to characterize indefinite metamaterials by an effective permittivity tensor.^{25,26} Our method is conversely a top-down approach that enables us to derive the effective index directly from the dispersion relationship. As a consequence it applies to both the homogeneous and diffractive regimes and allows us to calculate a dispersive complex effective index. The design of optimal flat lenses is thus guided by the effective index and figure of merit $\text{FOM} = |n/\kappa|$ maps obtained for various filling fractions of metal-dielectric films. The optical resolution of indefinite metamaterial lenses is directly derived from the complex band diagram and is shown to be limited by FOM and the focal distance. These results are successfully validated with a rigorous electromagnetic calculations based on a scattering-matrix method. Finally, realizable indefinite metamaterials with high FOM are shown to efficiently transport the evanescent waves to the rear face of the lens. This mechanism boosts the optical resolution beyond the diffraction limit, allowing us to make visible superresolved images up to a focal distance of one wavelength.

II. COMPLEX EFFECTIVE INDEX FOR HYPERBOLIC METAMATERIALS

Consider a periodic set of N slabs of silver and TiO₂ layers of thicknesses h_m and h_d and of complex relative permittivities $\bar{\epsilon}_m$ and $\bar{\epsilon}_d$ [Fig. 1(a)]. Silver films are placed at boundaries of the structure in order to benefit from surface plasmon polariton resonances. In the homogenization regime and for TM polarized electromagnetic waves propagating in the y direction, the effective permittivity tensor is characterized by the following diagonal elements:¹³

$$\bar{\epsilon}_x = \bar{\epsilon}_m f_m + \bar{\epsilon}_d f_d, \quad \bar{\epsilon}_y = \left(\frac{f_m}{\bar{\epsilon}_m} + \frac{f_d}{\bar{\epsilon}_d} \right)^{-1}, \quad (1)$$

where the filling factors in metal and dielectric are, respectively, $f_m = h_m/D$ and $f_d = h_d/D$, with $D = h_m + h_d$

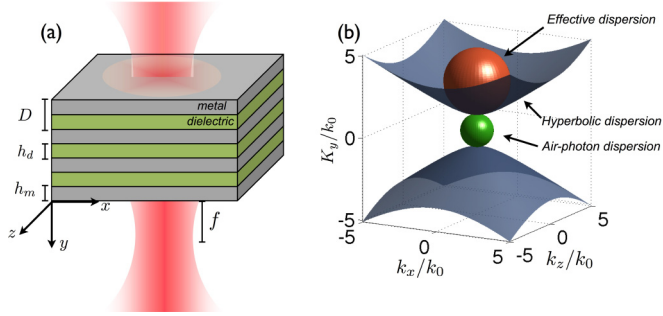


FIG. 1. (Color online) (a) Principle of light focalization by indefinite metamaterials consisting of a multilayer of metal and dielectric films. This hyperbolic lens focuses at the focal distance f . (b) Hyperbolic dispersion of an indefinite metamaterial; the green and red spheres represent, respectively, the dispersion relations of the air medium and of the effective medium.

being the lattice period. We denote by L the total thickness of the multilayer. For convenience, these diagonal complex elements are written in the following form: $\bar{\epsilon}_x = \epsilon_x(1 + i\sigma_x)$ and $\bar{\epsilon}_y = \epsilon_y(1 + i\sigma_y)$. Note that these effective permittivity components are valid in the long-wavelength limit (when $D/\lambda \ll 1$) and for small transverse wave vectors ($k_x/k_0 \ll 1$, where $k_0 = 2\pi/\lambda$).²⁷ Provided that the conditions given in Ref. 17 are satisfied, $\epsilon_y < 0$ and $\epsilon_x > 0$, and the hyperbolic relationship is $k_x^2/\bar{\epsilon}_y + \bar{k}_y^2/\bar{\epsilon}_x = (\omega/c)^2$. Here, k_x refers to the conjugate coordinate of x for the Fourier transform and reduces to a real number. We search for how to replace this anisotropic medium by an equivalent homogeneous medium of complex effective index \bar{n} that presents an isotropic photon dispersion $k_x^2 + \bar{k}_y^2 = (\bar{n}\omega/c)^2$ [Fig. 1(b)]. For a fixed frequency ω , we derive the complex wave vector \bar{k}_y in terms of a second-order Taylor expansion:

$$\bar{k}_y(k_x) = \bar{k}_y(0) - \bar{\gamma} k_x^2 / 2k_0, \quad (2)$$

where $\bar{\gamma} = -k_0(\partial^2 \bar{k}_y / \partial k_x^2)|_{k_x=0}$. This parabolic approximation of the hyperbolic dispersion allows us to replace an anisotropic medium by an isotropic one having the same complex curvature $\bar{\gamma} = 1/\bar{n}$. When weak optical absorption is considered, the real part of the effective index and the figure of merit FOM are

$$n = 1/\text{Re}(\bar{\gamma}), \quad (3)$$

$$\text{FOM} = |\text{Re}(\bar{\gamma})/\text{Im}(\bar{\gamma})|. \quad (4)$$

In the homogenization regime, the complex curvature reads $\bar{\gamma} = \sqrt{\bar{\epsilon}_x/\bar{\epsilon}_y}$, and the effective refractive index and FOM can be expressed in terms of the complex permittivity tensor elements:

$$n = -\frac{|\epsilon_y|}{\sqrt{\epsilon_x}}(1 + \sigma_x\sigma_y/2)^{-1}, \quad (5)$$

$$\text{FOM} = \left| \frac{2 + \sigma_x\sigma_y}{2\sigma_y - \sigma_x} \right|. \quad (6)$$

Equation (5) shows that the effective index is governed by the ratio $-|\epsilon_y|/\sqrt{\epsilon_x}$ and decreases when the material absorption increases. Despite these material losses, FOM is also seen to

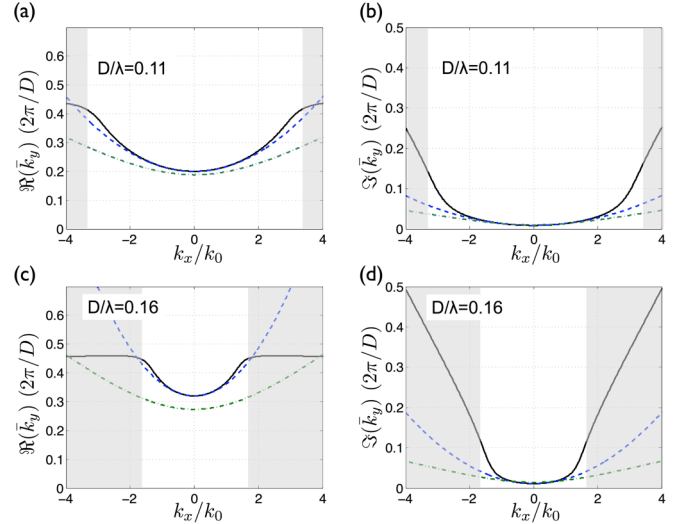


FIG. 2. (Color online) (a) Real and (b) imaginary parts of the equifrequency diagram in the (k_x, \bar{k}_y) space for $D/\lambda = 0.11$. (c) Real and (d) imaginary parts of the complex equifrequency diagram $D/\lambda = 0.16$. The solid, dashed, and dot-dashed curves represent, respectively, the exact band diagram, the paraxial expansion [Eq. (2)], and the homogenized approach [Eq. (1)]. These calculations are obtained for $h_m/h_d = 1$ and $\lambda = 380$ nm. The gray areas represent the angular photonic band gaps.

be maximal when $|2\sigma_y - \sigma_x|$ is minimal. As shown in Ref. 17, the dispersive properties of indefinite metamaterials strongly depends on the reduced frequency D/λ . As a consequence, the effective index and FOM given by Eqs. (5) and (6) only apply when $D/\lambda \ll 1$. Beyond the homogenization regime, it has been shown that the optical properties of metamaterials have to be retrieved from the exact photonic band diagram.²⁸ The parabolic approach can, however, be extended in the diffractive regime when the latter condition is not satisfied by computing the curvature $\bar{\gamma}$ from the complex band structure.²⁹ In this way, the real and imaginary parts of the complex curvature are, respectively, $\text{Re}(\bar{\gamma}) = -k_0[\partial^2 \text{Re}(\bar{K}_y)/\partial k_x^2]|_{k_x=0}$ and $\text{Im}(\bar{\gamma}) = -k_0[\partial^2 \text{Im}(\bar{K}_y)/\partial k_x^2]|_{k_x=0}$, where \bar{K}_y is the complex Bloch wave vector derived from the dispersion equation.^{29,30}

To validate this approach, the complex band diagram derived from the parabolic expansion given by Eq. (2) is compared to the exact one (Fig. 2). These curves are calculated at $\lambda = 380$ nm with $h_m/h_d = 1$ and for two reduced frequencies, $D/\lambda = 0.11$ and $D/\lambda = 0.16$, close to homogenization regime and in the diffractive regime, respectively. It is seen that a better fit is obtained in the long-wavelength limit with the parabolic approximation than with the band diagram derived from the effective permittivities of Eq. (1). Moreover, the parabolic dispersion matches almost perfectly the exact complex equifrequency curves until angular photonic band gaps appear for high- k vectors larger than $2k_0$. These results demonstrate that the parabolic approximation allows us to study light focalization of subwavelength sources and, consequently, to optimize the optical resolution.

According to Eqs. (3) and (4), the effective refractive index and FOM can now be systematically explored for various wavelengths and metal-dielectric filling factors (Fig. 3). We

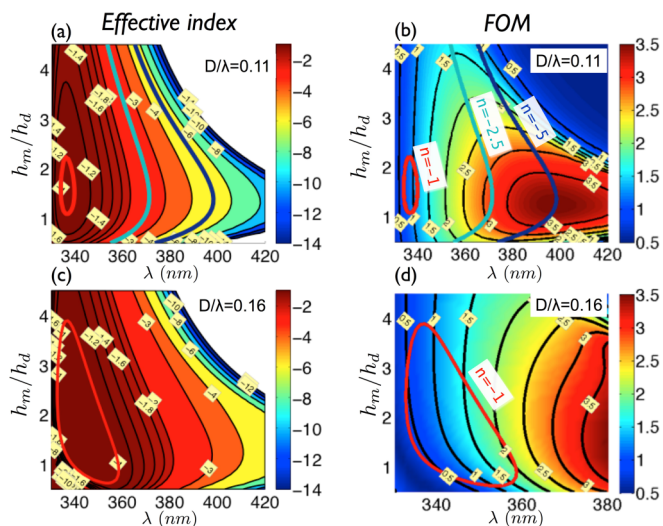


FIG. 3. (Color online) Effective index and FOM with respect to the wavelength and the metal-dielectric ratio for (a) and (b) $D/\lambda = 0.11$ and (c) and (d) $D/\lambda = 0.16$. Equi-index curves of -1 , -2.5 , and -5 effective indices (red, green, and blue curves) are superposed in the FOM maps.

consider again two reduced frequencies, $D/\lambda = 0.11$ and $D/\lambda = 0.16$, and to be as realistic as possible, the dispersive complex permittivities of silver and TiO_2 are taken into account.^{31,32} The effective index is shown to range from -1 to about -10 for wavelengths between 330 and 420 nm, and it is also redshifted when the reduced frequency increases, leading to a wider -1 equi-index curve for $D/\lambda = 0.16$. FOM is seen to be optimal around $\lambda = 400$ nm and when h_m/h_d is close to 1.3 . From these maps, we conclude that the best flat lens made with indefinite metamaterials with a -1 refractive index is obtained for FOM = 2 when the following parameters hold: $D/\lambda = 0.16$, $\lambda = 358$ nm, $h_m/h_d = 1.07$. These parameters lead to silver and TiO_2 thicknesses of $h_d = 28$ nm and $h_m = 30$ nm, which are very close to the parameters used by Xu *et al.* in their experimental demonstration.¹⁹ Looking for lower optical losses leads to a lens with FOM as high as 4, obtained for $D/\lambda = 0.11$ at $\lambda = 398$ nm and $h_m/h_d = 1.28$. However, in that case, the hyperbolic flat lens is characterized by an effective index of -5 . We finally underline that the relatively smooth variation of the effective index and the figure of merit with respect to any change of the aspect ratio is probably a sign that the optical properties are resistant to disorder.

III. OPTICAL RESOLUTION OF HYPERBOLIC METAMATERIAL LENSES

In order to compare the optical efficiency of these -1 and -5 effective index metamaterials, referred to as $I_M^{(-1)}$ and $I_M^{(-5)}$, respectively, we derive a model that directly links their FOM to the optical resolution. We assume an incident Gaussian beam of waist W that impinges the input interface. After propagating through the lens, whose thickness is L , the transmitted signal calculated at a distance y far away from the output interface

reads

$$U(x, y) = \int_{-\infty}^{\infty} A(k_x) T(k_x) t_0(k_x, y) e^{ik_x x} dk_x \quad (7)$$

where $t_0(k_x, y) = e^{iy\sqrt{k_0^2 - k_x^2}}$ is the transfer function in the output air medium and $A(k_x) = W_0/(2\sqrt{\pi}) \exp[-(k_x W/2)^2]$ is the spectrum of the incident Gaussian beam in the k space. The multilayer transmission coefficient $T(k_x)$ splits into a singular part $T^s(k_x) = \sum_p t_p/(k_x - \bar{k}_x^{(p)})$, where $\bar{k}_x^{(p)}$ and t_p are the poles and the residues associated with optical resonances, and a regular part $T^r(k_x)$. Since this holomorphic function accounts for both the phase and the optical absorption accumulated by the signal when propagating through the metamaterial slab, we assume that it is driven by the complex Bloch wave vector: $T^r(k_x) = e^{i\bar{K}_y(k_x)L}$. The use of the parabolic expansion of $\bar{K}_y(k_x)$ allows T^r to be expressed in terms of the effective index and FOM:

$$T^r(k_x) = e^{i\bar{K}_y(0)L} e^{-\frac{k_x^2}{2k_0} \frac{L}{|\text{FOM}|}} e^{-i\frac{k_x^2}{2k_0} \frac{L}{n}}. \quad (8)$$

An image is obtained when the focalization power provided by the lens cancels out the optical diffraction in air, i.e., when the total phase vanishes at the focal distance f . As shown in Ref. 17, the paraxial approximation applied to t_{air} leads to $f = -L/n$, where n is the effective index defined in Eq. (3) and $L = DN + h_m$ is the lens thickness. Finally, the focalized beam is the sum of a resonant field $U^s(x, f)$ linked to $[T^s(k_x)]$ and a regular field $U^r(x, f)$, given by

$$U^r(x, f) = \int_{-\infty}^{\infty} A(k_x) |T^r(k_x)| |t_0(k_x, f)| e^{ik_x x} dk_x. \quad (9)$$

Perfect resolution implies that the transfer function product $|T^r(k_x)| |t_0(k_x, f)| = 1$ for all high- k waves, where in that case $|t_0(k_x, f)| = e^{-f\sqrt{k_x^2 - k_0^2}}$. However, Eq. (10), derived from Eq. (8), shows that evanescent waves (for $k_x > k_0$) are reduced rather than amplified inside indefinite metamaterials, contrary to what would be expected for a perfect lens:¹

$$|T^r(k_x)| = e^{-\text{Im}[\bar{K}_y(0)]L} e^{-\frac{k_x^2}{2k_0} \frac{L}{|\text{FOM}|}}. \quad (10)$$

As a consequence of this description, the optimal transport of subwavelength details requires a large FOM, but it is limited by the focal distance. We apply these results to the optimized indefinite metamaterials $I_M^{(-1)}$ and $I_M^{(-5)}$ of the respective effective indices -1 and -5 . The exact transfer function computed with a rigorous modal transfer-matrix method³³ is compared to the total transfer function $T^p = |T^r(k_x)| |t_0(k_x, f)|$ derived from the parabolic approximation of Eq. (10) (Fig. 3). For that purpose, the focal distance is initially kept to half a wavelength ($f = \lambda/2$) by using the convenient number of lattice periods, and a Gaussian beam of subwavelength waist $W_0 = \lambda/20$ is launched toward the input lens interface. Figures 3(a) and 3(d) show that the parabolic transfer function T^p agrees well with the rigorous one and that its slope is reduced when FOM increases. The sharp oscillations observed around $k_x = \pm 1.2k_0$ correspond to poles of the singular part. These resonances, associated with surface plasmon polaritons (SPPs) such as resonances bounded at the rear lens interface, are, however, only activated for $I_M^{(-5)}$ [Figs. 4(c) and 4(f)]. Despite the fact that these surface modes are not caught by the parabolic

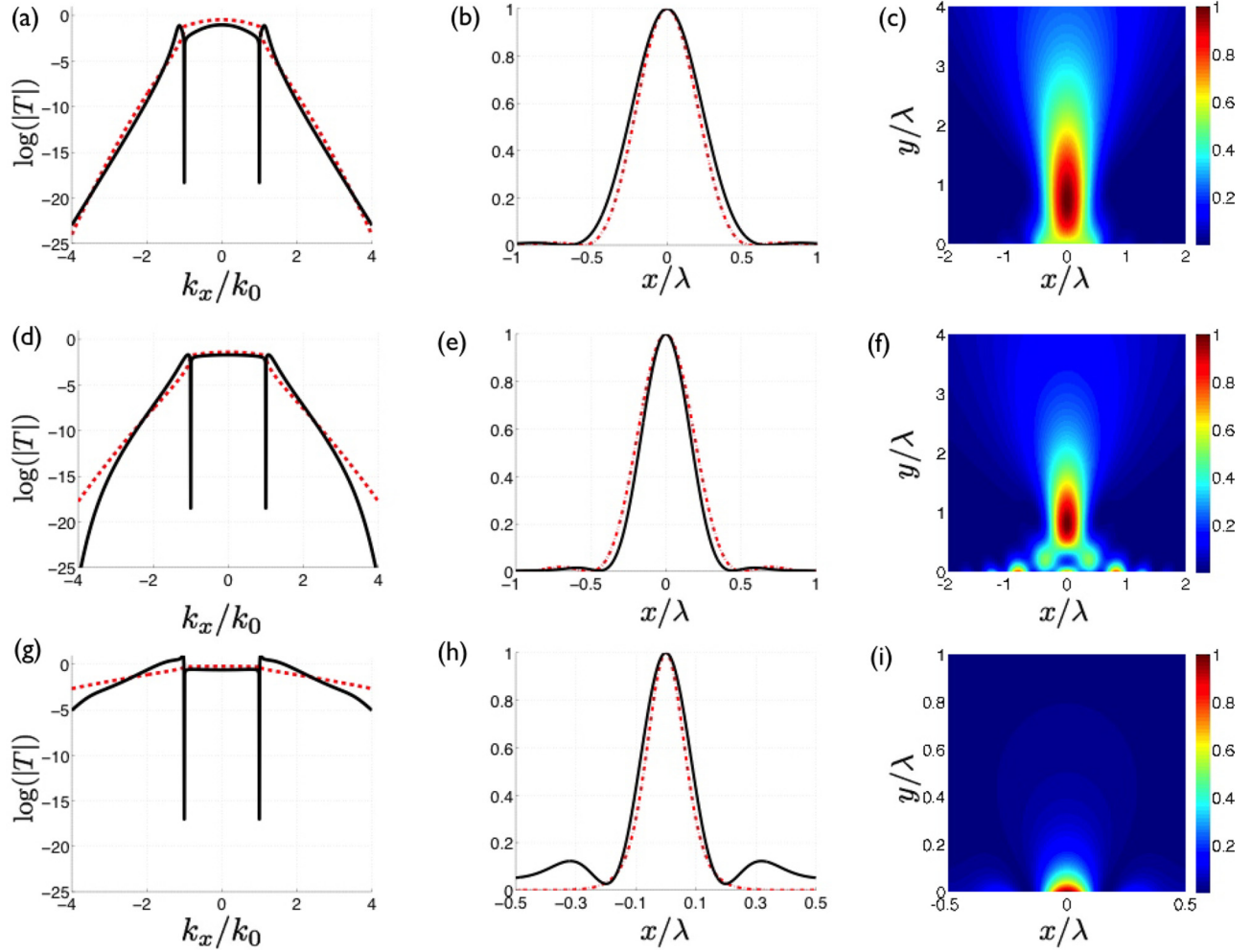


FIG. 4. (Color online) Logarithm of the transfer functions, intensity profiles obtained at the focal distance, and maps of focalized beams. The solid and dashed curves correspond, respectively, to the exact transfer function and the paraxial one T^P . (a)–(c) and (d)–(f) are obtained for $f = \lambda/2$ with $I_M^{(-1)}$ and $I_M^{(-5)}$, respectively. (g)–(i) correspond to $I_M^{(-5)}$ for $f = \lambda/18$.

transfer function T^P , the derived intensity profiles match the rigorous computations almost perfectly. This demonstrates the validity of the description of indefinite metamaterials in terms of the effective complex index [Figs. 4(b), 4(e), and 4(h)]. Finally, the full width at half maximum (FWHM) calculated for this focal distance shows that a subwavelength resolution of $\lambda/2.7$ is achieved for $I_M^{(-5)}$ (with a FOM of 4) while the optical resolution of $I_M^{(-1)}$ is limited to $\lambda/1.9$ since its $\text{FOM} = 2$. A high FOM allows us to efficiently transport both the propagating and evanescent waves, with the latter particularly boosting the resolution. This mechanism enhances the optical resolution by optimizing the regular field $U^r(x, f)$ and increases the contribution of the singular field $U^s(x, f)$. A maximal resolution of $\lambda/6$ is reached for $I_M^{(-5)}$ when the image is focused at the output lens interface [Figs. 3(g)–3(i)]. Beyond this canalization regime, superresolution persists as long as the focal distance is smaller than λ , showing the crucial impact of high FOM and SPP-like resonances (Fig. 5). The lower FOM of the $I_M^{(-1)}$ device only enables superresolution for a short focal distance of $\lambda/3$, which corresponds to a multilayer of three lattice periods. Beyond this distance, subwavelength details carried by high- k components are irreversibly lost because of the optical losses.

IV. CONCLUSIONS

In conclusion, we have demonstrated that indefinite metamaterials characterized by an anisotropic permittivity tensor

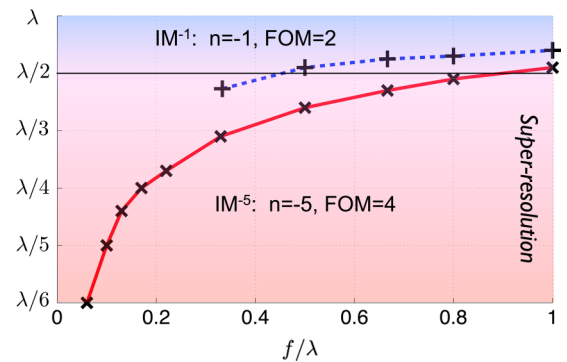


FIG. 5. (Color online) Optical resolution with respect to the focal distance in units of λ for $I_M^{(-1)}$ (dashed curve) and $I_M^{(-5)}$ (solid curve). Superresolution (red area) is obtained with $I_M^{(-5)}$ as long as the focal distance is smaller than one wavelength. Points are obtained with the rigorous transfer-matrix method.³³

are equivalent to isotropic homogeneous metamaterials with a complex negative effective index. This effective refractive index and its associated absorption constant are extracted by the use of a parabolic expansion from the complex Bloch diagram. This approach applies in both the homogenization and diffractive regimes and gives maps of effective index and FOM for various metal-dielectric compositions and wavelengths. This systematic study allows the design of optimal lenses based on indefinite metamaterials. We have in addition developed a semianalytical theory that links the FOM to the optical resolution of such lenses. These results, validated by scattering matrix computations, show that indefinite metamaterials of large FOM are required to efficiently transport high- k components of the signal. Subwavelength resolution is then attributed to a SPP-like resonance-assisted mechanism

rather than the *amplification* of evanescent waves theorized for left-handed metamaterials. Finally, we show that a feasible hyperbolic lens with a -5 effective index can outperform the optimal lens with a -1 effective index by allowing visible light focalization (at $\lambda = 400$ nm) together with superresolution for focal distances as large as one wavelength. Any further study of these structures should probably take into account the impact of nonlinearities such as nonlinear light absorption,¹⁹ the Kerr effect,³⁴ and nonlocality effect.³⁵ The physics of indefinite metamaterials is far from being exhausted, and as new applications for these structures arise,³⁶ we hope the present work will be useful in many as yet unforeseen ways.

We would like to thank K. Vynck and C. Sauvan for helpful discussions.

-
- ¹J. B. Pendry, *Phys. Rev. Lett.* **85**, 3966 (2000).
²N. I. Zheludev and Y. S. Kivshar, *Nat. Mater.* **11**, 917 (2012).
³V. P. Drachev, V. A. Podolskiy, and A. V. Kildishev, *Opt. Express* **21**, 15048 (2013).
⁴D. R. Smith and D. Schurig, *Phys. Rev. Lett.* **90**, 077405 (2003).
⁵J. Sun, J. Zeng, and N. M. Litchinitser, *Opt. Express* **21**, 14975 (2013).
⁶S. A. Biehs, M. Tschikin, R. Messina, and P. Ben-Abdallah, *Appl. Phys. Lett.* **102**, 131106 (2003).
⁷Y. Guo and Z. Jacob, *Opt. Express* **21**, 15014 (2013).
⁸X. Yang, J. Yao, J. Rho, X. Yin, and X. Zhang, *Nat. Photonics* **6**, 450 (2012).
⁹I. I. Smolyaninov, Y.-J. Hung, and C. C. Davis, *Science* **315**, 1699 (2007).
¹⁰Z. Liu, H. Lee, X. Yi, C. Sun, and X. Zhang, *Science* **315**, 1686 (2007).
¹¹E. E. Narimanov and V. M. Shalaev, *Nature (London)* **447**, 266 (2007).
¹²P. A. Belov, C. R. Simovski, and P. Ikonen, *Phys. Rev. B* **71**, 193105 (2005).
¹³P. A. Belov and Y. Hao, *Phys. Rev. B* **73**, 113110 (2006).
¹⁴M. Scalora *et al.*, *Opt. Express* **15**, 508 (2007).
¹⁵M. J. Bloemer, G. D'Aguanno, M. Scalora, N. Mattiucci, and D. de Ceglia, *Opt. Express* **16**, 19342 (2008).
¹⁶N. Mattiucci, G. D'Aguanno, M. Scalora, M. J. Bloemer, and C. Sibilia, *Opt. Express* **19**, 17517 (2009).
¹⁷J. Benedicto, E. Centeno, and A. Moreau, *Opt. Lett.* **37**, 4786 (2012).
¹⁸E. Verhagen, R. de Waele, L. Kuipers, and A. Polman, *Phys. Rev. Lett.* **105**, 223901 (2010).
¹⁹T. Xu, A. Agrawal, M. Abashin, K. J. Chau, and H. J. Lezec, *Nature (London)* **497**, 470 (2013).
²⁰K. Vynck, D. Felbacq, E. Centeno, A. I. Căbuz, D. Cassagne, and B. Guizal, *Phys. Rev. Lett.* **102**, 133901 (2009).
²¹C. R. Simovski, *Opt. Spectrosc.* **107**, 726 (2009).
²²M. G. Silveirinha, *Phys. Rev. B* **75**, 115104 (2007).
²³D. R. Smith and J. B. Pendry, *J. Opt. Soc. Am. B* **23**, 391 (2006).
²⁴J. B. Pendry, A. J. Holden, D. J. Robbins, and W. J. Stewart, *IEEE Trans. Microwave Theory Tech.* **47**, 2075 (1999).
²⁵I. Iorsh, A. Poddubny, A. Orlov, P. Belov, and Y. S. Kivshar, *Phys. Lett. A* **376**, 185 (2012).
²⁶O. Kidwai, S. V. Zhukovsky, and J. E. Sipe, *Phys. Rev. A* **85**, 053842 (2012).
²⁷X.-B. Kang, W. Tan, and Z.-G. Wang, *Opt. Commun.* **284**, 4237 (2011).
²⁸T. Paul, C. Rockstuhl, C. Menzel, and F. Lederer, *Phys. Rev. B* **79**, 115430 (2009).
²⁹M. Bergmair, M. Huber, and K. Hingerl, *Appl. Phys. Lett.* **89**, 081907 (2006).
³⁰R. Pollès, E. Centeno, J. Arlandis, and A. Moreau, *Opt. Express* **19**, 6149 (2011).
³¹J. R. DeVore, *J. Opt. Soc. Am.* **41**, 416 (1951).
³²E. D. Palik, *Handbook of Optical Constants of Solids* (Academic, New York, 1991).
³³F. Krayzel, R. Pollès, A. Moreau, M. Mihailovic, and G. Granet, *J. Eur. Opt. Soc.* **5**, 10025 (2010).
³⁴N. Katte, J. W. Haus, P. Powers, A. Sarangan, J. Gao, and M. Scalora, *J. Opt. Soc. Am. B* **28**, 2277 (2011).
³⁵W. Yan, N. Asger Mortensen, and M. Wubs, *Opt. Express* **21**, 15026 (2013).
³⁶S.-A. Biehs, M. Tschikin, and P. Ben-Abdallah, *Phys. Rev. Lett.* **109**, 104301 (2012).